RSC Advances

PAPER

View Article Online
View Journal | View Issue

Cite this: *RSC Adv.*, 2023, **13**, 32558

An efficient biosensor using a functionalized microneedle of Cu_2O-based CoCu-LDH for glucose detection†

Jialei Zhu, Fuqin Wang, Jiaying Chen and Chang Liu*

Glucose detection with small and micro volume sampling has recently received increasing attention in monitoring personal health. Herein, a cauliflower-type cluster of Cu_2O nanoparticles (NPs) was directly deposited on the tip surface of a stainless steel acupuncture needle electrode (ANE) by electrochemical deposition, and then this pre-formed cuprous basis was used to further prepare the neatly arranged CoCu-layered double hydroxide (CoCu-LDH) nanosheets that interconnected to form nano-sized pores in the range from 100 to 500 nm. The microstructure and spectral characteristics of the surface modification materials were comprehensively characterized by FE-SEM, EDS, XRD, FT-IR and TEM. Cu_2O-based CoCu-LDH composites with special morphology had been proven to accelerate the rate of electron transport and provide more available active centers, and moreover, the mixed valence of Cu/Co induced an excellent synergism for the electrocatalytic oxidation of glucose. As a result, CoCu-LDH/Cu_2O/ANE as a sensitive glucose probe exhibited two wider linear ranges of 0.03–0.40 mM and 0.40–6.00 mM, with sensitivities of 116.13 μA mM^{-1} and 52.08 μA mM^{-1}, respectively, and the detection limit as low as 0.46 μM (S/N = 3). The response time only took 3 s and it kept working stably in the interference of ascorbic acid (AA), dopamine (DA), uric acid (UA), and Cl^-. In the stability test, the CoCu-LDH/Cu_2O/ANE sensor exhibited a stable monitoring sensitivity after 15 days. Finally, the CoCu-LDH/Cu_2O/ANE sensor had been successfully applied to glucose analysis in human serum, proving that our design was an attractive strategy for developing a portable, minimally invasive, and low-cost non-enzymatic electrochemical glucose sensing platform.

Received 1st September 2023
Accepted 23rd October 2023

DOI: 10.1039/d3ra05957j

rsc.li/rsc-advances

Introduction

Diabetes is a metabolic disease linked to high blood glucose levels that can cause damage to a variety of organs and tissues in the body, including the heart, kidneys, eyes and nerves.[1–3] Regular monitoring of glucose in the blood is important to control diabetes and its complications.[4,5] Although different methods including spectrophotometric, chromatographic and electrochemical-based techniques have been used for glucose detection, the aforementioned two techniques are not suitable for daily glucose testing because of their heavy equipment and complicated operation.[6–8] Thus, electrochemical sensors have received wide attention due to some advantages of rapid detection, low cost, simplicity, environmental friendliness, high sensitivity, fast response time and good selectivity.[9–11]

The electrochemical sensors are mainly based on enzymatic and non-enzymatic mechanisms of action.[12,13] Loading enzymes on the electrode for blood glucose monitoring is widely used because of inherent selectivity and sensitivity, but some deficiencies of poor stability, high fabrication cost and complex process of enzyme immobilization are very difficult to overcome.[14,15] Hence, non-enzymatic glucose electrochemical sensors opened up a new track by using direct redox reactions between glucose and electrodes.[16] Among the reported electrochemical sensors, modified electrodes with transition metal oxides (TMOs) such as ZnO,[17,18] NiO,[19] CuO,[20] Cu_2O,[21,22] Co_3N[23] and Co_3O_4 (ref. 24) exhibit various advantages even beyond other noble metal or graphene sensors, especially the unique d-orbital properties that enhance their electrocatalytic activity.[25,26] Besides, some TMOs have a tendency to form layered double hydroxides (LDH) in alkaline media, which induces an outstanding performance for electrocatalytic oxidation of glucose.[27,28] Here, the LDH structure usually consists of a positively charged metal hydroxide laminate and an interlayer containing water molecules and a large number of anions, exhibiting a structure similar to a "house of cards".[29] By taking advantage of the special structure of LDH, TMOs get the inherent anion exchange properties, even more effectively under charged situations.[30]

To date, quite a few studies on LDH synthesis methods have been reported, such as *in situ* co-precipitation, ion exchange,

College of Pharmacy, Jinzhou Medical University, Jinzhou, Liaoning, P. R. China. E-mail: liuchang@jzmu.edu.cn

† Electronic supplementary information (ESI) available. See DOI: https://doi.org/10.1039/d3ra05957j

roasting reconstruction, solvothermal methods and electrochemical deposition.[31] Traditional preparation methods for LDH films often suffer from weak bonding between LDH materials and the conductive substrate, which results in poor mechanical and electrochemical properties.[32] By comparison, electrochemical deposition does not require the addition of suitable conductive agents and binders as in the coating method, thus making it significant for improving the electrochemical property and the electrode utilization of LDH film electrodes.[33] The preparation mechanism has been demonstrated as follows:

$$NO^{3-} + H_2O + 2e^- = NO^{2-} + 2OH^- \quad (1)$$

While electrochemical deposition is based on the reduction properties of anions in solution (NO_3^- for example), OH^- generated in the reduction reaction will combine with metal ions in solution to obtain LDH products and then attach to the conductive substrate to form a thin film.[34] However, the poor film-forming nature of LDH leads to its not being easily prepared directly on the conductive substrates.[35] Therefore, to remedy these deficiencies, suitable materials need to be designed as the substrate to improve the conductivity and film-forming properties of LDH.[36]

Actually, traditional electrodes, such as glassy carbon electrodes, gold electrodes, and indium tin oxide glass electrodes, have been regarded by many researchers as the preferred substrates for LDH construction.[37] But the large substrates available are not adequate for the demands of small and micro volume sample detection and portable sensors fabrication. So microneedle technology has been developed, which provides a more convenient and comfortable experience throughout percutaneous puncture sampling and detection.[38] Subsequently, the stainless steel acupuncture needle electrode (ANE), a flexible microneedle electrode, has been key in the progress of small biomolecule detection, such as the detection of epinephrine,[39] dopamine,[40] catecholamines,[41] adenosine triphosphate,[42] ascorbic acid,[43] nitrate[44] and polyphenols.[45]

In this work, a novel three-dimensional layer of cauliflower-type Cu_2O nanoparticles (NPs) was forcibly formed on the ANE surface, and then CoCu-LDH nanosheets were designed to decorate the surface of Cu_2O NPs. Expectedly, stable, porous and neatly arranged CoCu-LDH nanoarrays were obtained by cyclic voltammetry (CV) treatment in an alkaline solution (Scheme 1).

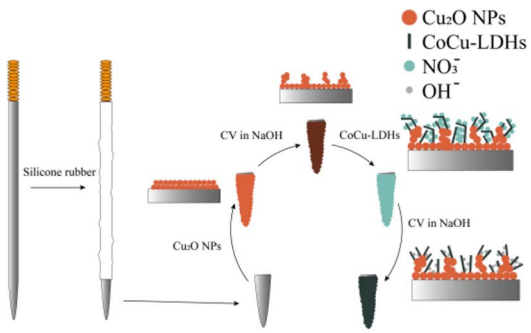

Scheme 1 The fabrication of CoCu-LDH/Cu_2O/ANE.

The morphology and composition of hybridized nanocomposites were characterized by FE-SEM, EDS, XRD, FT-IR and TEM. The electrocatalytic ability of CoCu-LDH/Cu_2O/ANE for glucose oxidation was evaluated by CV, electrochemical impedance spectroscopy (EIS) and chronoamperometry. The results showed that, unlike the corresponding monometallic materials, the Co/Cu bimetal possessed a special electrochemical activity on glucose oxidation due to the bimetallic synergism and the improved electrical conductivity of modified ANE. The electron transfer rates of glucose on CoCu-LDH/Cu_2O/ANE were faster than those on bare ANE, Cu_2O/ANE, and CoCu-LDH/Cu_2O modified ANE before CV treatment (CoCu-LDH/Cu_2O/ANE). The sample detection further confirmed the feasibility of the glucose sensing platform based on CoCu-LDH/Cu_2O/ANE.

Experimental

Instruments

A field emission scanning electron microscope (FE-SEM Sigma 300, Zeiss, Germany) equipped with an energy dispersive spectroscopy (EDS) probe was used to investigate the surface morphology and chemical composition of hybridized nanocomposites and ANE. The X-ray diffraction curves were recorded by TDM-10 Powder X-ray diffraction (XRD, China) with a Cu Kα radiation diffractometer (40 kV, 30 mA) to determine the crystal structures of CoCu-LDH/Cu_2O before and after CV treatment in the alkaline solution. FT-IR spectra of Cu_2O, untreated CoCu-LDH/Cu_2O and treated CoCu-LDH/Cu_2O were obtained on an IRAffinity-1 spectrometer (Shimadzu, Japan). The morphology and lattice fringes analyses of the CoCu-LDH were conducted using transmission electron microscope (TEM, Jem-2100F) including high resolution transmission electron microscope (HRTEM) and the selected area electron diffraction (SAED) pattern. Electrochemical measurements were performed using a CHI660E electrochemical workstation (Chenhua, Shanghai, China) in a typical three-electrode system. A bare or modified ANE was used as the working electrode. A KCl-saturated Ag/AgCl electrode and a platinum wire electrode (Pt wire) were used as the reference and counter electrodes, respectively. The glucose in human serum samples was determined by the self-made electrode and Sinocare SG-103 blood glucose meter and then compared with the hospital test results.

Chemicals

D-(+)-glucose (Glu), dopamine hydrochloride (DA > 98%), ascorbic acid (AA ≥ 99%), uric acid (UA ≥ 99%), copper sulfate pentahydrate ($CuSO_4 \cdot 5H_2O$ ≥ 99%), glacial acetic acid (CH_3COOH ≥ 99.8%), cobalt nitrate hexahydrate ($Co(NO_3)_2 \cdot 6H_2O$ ≥ 99%), sodium nitrate ($NaNO_3$ ≥ 99%), sodium hydroxide (NaOH ≥ 96%), sodium chloride (NaCl ≥ 99.5%), and potassium chloride (KCl ≥ 99.5%) were purchased from Aladdin Biochemical Technology Co. Ltd. Stainless steel acupuncture needles (size 0.25 × 40 mm) were purchased from Suzhou

Medical Appliance Factory Co. Ltd. (Suzhou, China). Silicone rubber obtained from Liyang Kangda Chemical Co. Ltd (Liyang, China) was used as the insulating and sealing material. All other reagents were at least analytical reagent grade and could be used without further purification. The solutions were prepared using deionized water.

Methods

Fabrication of CoCu-LDH/Cu_2O/ANE

The ANE was processed separately in anhydrous ethanol and deionized water with ultrasonic cleaning for 10 min then dried. As shown in Scheme 1, the pretreated ANE was electrically insulated by coating an epoxy resin layer on the needle surface except for the 2.0 mm needle tip which was exposed as the sensing area. Cu_2O NPs were subsequently electrodeposited by a constant potential of −0.5 V in a solution of 10% acetic acid and 0.1 M copper sulfate. Then, to form cauliflower-type Cu_2O NPs, the electrode was immersed in 0.1 M NaOH solution and treated using CV method scan for 20 cycles at a potential range of −0.5 to 0.3 V in a scan rate of 100 mV s^{-1}. The freshly prepared Cu_2O/ANE was further modified by electrodeposition at −0.6 V in the solution of 0.05 M cobalt nitrate and 0.1 M sodium nitrate. After that, a primary model of CoCu-LDH/Cu_2O/ANE was obtained, but it must be electrochemically activated in 0.1 M NaOH solution at the potential range of −0.1 to 0.8 V for 40 cycles to fabricate CoCu-LDH/Cu_2O/ANE before use.

Electrochemical measurements

Electrochemical measurements include the electrochemical characterization of electrode properties and glucose detection. First, the electrochemical properties of the electrode were characterized using EIS and CV methods. EIS was performed using 20 mmol L^{-1} $K_3Fe(CN)_6/K_4Fe(CN)_6$ (0.1 mol L^{-1} KCl) as the supporting electrolyte with a bias potential of 0.24 V and a frequency range of 0.1–10^6 Hz. Second, the amperometric method was used to test glucose standard solutions and human serum samples in a continuously stirred 0.1 M NaOH solution. The test potential was 0.55 V.

Results and discussion

Structural and morphological analyses

The bare ANE, Cu_2O/ANE, untreated CoCu-LDH/Cu_2O and treated CoCu-LDH/Cu_2O were characterized by FE-SEM. As shown in Fig. 1A–C, the bare ANE had a very smooth surface with a bright metallic luster, which made it difficult for CoCu-LDH to be directly modified on the surface of ANE. So the cauliflower-type Cu_2O NPs were modified to provide a rough substrate for a follow-up operation (Fig. 1D–F). As we expected, a relatively broad and flat surface could be observed in Fig. 1G and demonstrated success in the primary model of CoCu-LDH modification. Compared to the haphazard structure of CoCu-LDH nanosheets in Fig. 1H and I, considerable morphological changes occurred after CV treatment (Fig. 1K and L). It meant that the interconnected CoCu-LDH nanosheets tended to form ordered and hierarchical arrays in the main pore sizes of 100–500 nm. The special structure of CoCu-LDH nanosheets could be a key factor in facilitating glucose diffusion. Fig. 1M showed the FE-SEM images of CoCu-LDH/Cu_2O/ANE in a direction parallel to the ANE, in which it showed an obvious three-layer structure with a total thickness of Co-LDH/Cu_2O in 90 μm. The outer layer of the fabricated ANE was about 3 μm and consisted of CoCu-LDH. Moreover, the interlayer of joining CoCu-LDH to ANE substrate remained Cu_2O nanocluster structures, plus overlaying CoCu-LDH nanosheets to form spiny balls (Fig. 1N and O).

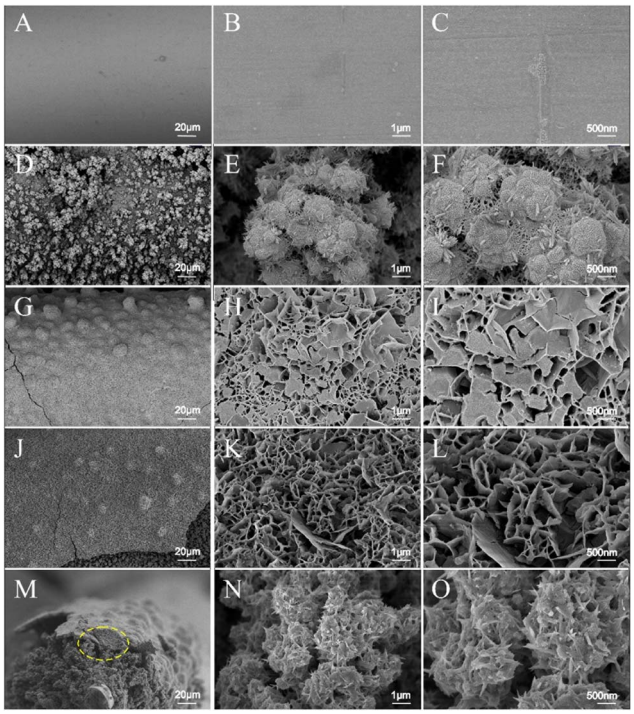

Fig. 1 FE-SEM images of bare ANE (A–C), Cu_2O/ANE (D–F), untreated CoCu-LDH/Cu_2O/ANE (G–I), treated CoCu-LDH/Cu_2O/ANE (J–L), treated CoCu-LDH/Cu_2O/ANE in a direction parallel to the ANE (M) and the enlarged portion circled in yellow (N and O).

EDS results revealed that Fe, Cr, Ni, and Co were the matrix materials of ANE (Fig. 2A). Compared with the bare ANE, two elements of Cu and O were distributed in the Cu_2O/ANE with a content percentage of 2 : 1, and the Co element that owes to the impurity of ANE disappeared completely. After the electrochemical deposition of $Co(OH)_2$ nanosheets on the Cu_2O/ANE, typical Co peaks re-appeared on the EDS patterns, and the Cu peak could still be observed but with content decrease. Besides that, the content percentage of Co to O remained at 1 : 2 after the CV treatment, indicating that the CV treatment only changed the interlayer composition of CoCu-LDH nanosheets. All EDS results shown here were completely consistent with the previous FE-SEM results and further confirmed that CoCu-LDH structure had been prepared successfully.

As shown in Fig. 2B, the changes in the phase and surface composition of CoCu-LDH/Cu_2O before and after CV treatment were further investigated by XRD. The XRD pattern of unteated

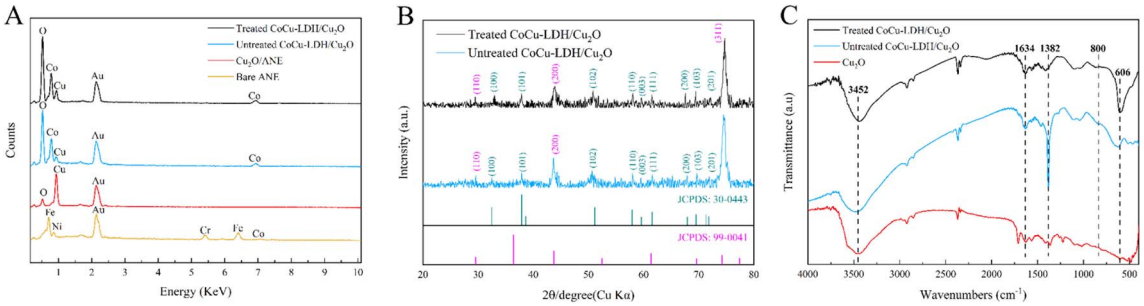

Fig. 2 (A) The EDS results of bare ANE, Cu_2O/ANE, untreated CoCu-LDH/Cu_2O/ANE, treated CoCu-LDH/Cu_2O/ANE, (B) X-ray diffraction patterns of untreated CoCu-LDH/Cu_2O and treated CoCu-LDH/Cu_2O porous nanohybrid array, and (C) FT-IR spectra of Cu_2O, untreated CoCu-LDH/Cu_2O and treated CoCu-LDH/Cu_2O porous nanohybrid array.

CoCu-LDH/Cu_2O showed clear diffraction peaks at 2θ angles of 32.48°, 37.88°, 50.48°, 57.98°, 59.56°, 61.56°, 67.88°, 69.68° and 71.92°, while the XRD results of treated CoCu-LDH/Cu_2O approached the results mentioned above and showed clear diffraction peaks at 2θ angles of 32.92°, 37.90°, 50.84°, 58.02°, 59.56°, 61.48°, 67.58°, 69.48° and 71.96°. All these diffraction peaks could be attributed to the (100), (101), (102), (110), (003), (111), (200), (103) and (201) crystal planes of hexagonal β-$Co(OH)_2$ (JCPDS No. 30-0443),[46] which suggested that the CV treatment only changed the interlayer composition of CoCu-LDH nanosheet, as the conclusion deduced by FE-SEM and EDS tests. There were, in addition, diffraction peaks at 2θ angles of 29.42°, 43.86° and 74.68° attributing to the (110), (200) and (311) crystal planes of Cu_2O (JCPDS No. 99-0041).[47]

The FT-IR spectra of Cu_2O, untreated CoCu-LDH/Cu_2O and treated CoCu-LDH/Cu_2O were shown in Fig. 2C. The absorption peak at 3452 cm^{-1} was attributed to the stretching vibration of the water molecule and the free OH group from hydroxide,[48] while the sharp peak at 1634 cm^{-1} could also be attributed to the bending vibration of the interlayer water molecule.[49,50] For the untreated CoCu-LDH/Cu_2O sample, the peak observed at 1382 cm^{-1} was attributed to the N–O stretching vibration of NO_3^- present in the interlayer space.[51] The weakened absorption peak of treated CoCu-LDH/Cu_2O at 1382 cm^{-1} suggested that CV treatment had significantly reduced NO_3^- content in the interlayer space of CoCu-LDH nanosheets, which was consistent with the results given by EDS and XRD. In addition, the weak absorption peaks below 800 cm^{-1} could be related to the stretching and bending vibrations of metal–oxygen bonds.[52,53]

To better characterize the composition and crystallinity, the surface layer of CoCu-LDH/Cu_2O was peeled off by ultrasonic treatment and subjected to the TEM measurement (Fig. 3A and B), in which the microstructure of CoCu-LDH nanosheet was much more distinct than that provided by FE-SEM. Combining the results provided by HRTEM and SAED measurements (Fig. 3C and D), the lattice fringe of 0.17 nm was contributed to the (102) plane of hexagonal β-$Co(OH)_2$ (JCPDS No. 30-0443),[54] while the lattice spacing of 0.30 nm was matched with the (110) plane of Cu_2O (JCPDS No. 99-0041).[55,56] Obviously, the HRTEM results were consistent with the corresponding XRD results, further confirming the microstructure and compositions of CoCu-LDH.

Electrochemical characteristics of CoCu-LDH/Cu_2O/ANE

The electrochemical characteristics of ANE and its fabricated form were evaluated by the CV technique in 0.1 M NaOH electrolyte solution. Fig. 4A showed the CV curves of bare ANE, Cu_2O/ANE, $Co(OH)_2$/ANE, and CoCu-LDH/Cu_2O/ANE with a potential range of −0.1 to 0.8 V and a scan rate of 30 mV s^{-1}. It could be seen that no significant redox peaks appeared for bare ANE and Cu_2O/ANE. In contrast, redox peak currents of 3.25 μA and 1.30 μA could be observed for $Co(OH)_2$/ANE at potentials of 0.20 V and 0.55 V, respectively. Incorporating Cu_2O NPs into CoCu-LDH significantly facilitated current growth 40–50 times at potentials of 0.23 V and 0.56 V, which mainly originated from the redox reactions of Cu^{1+}/Cu^{2+}, Cu^{2+}/Cu^{3+}, Co^{2+}/Co^{3+} and Co^{3+}/Co^{4+}, by supported OH^- anions in the alkaline electrolyte according to the following reactions:[57,58]

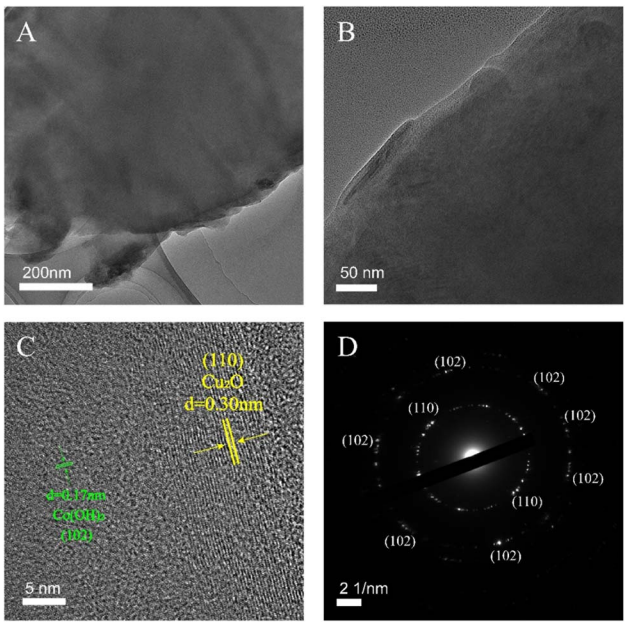

Fig. 3 The TEM image of CoCu-LDH (A), the HRTEM images of CoCu-LDH (B and C), and the SAED image of CoCu-LDH (D).

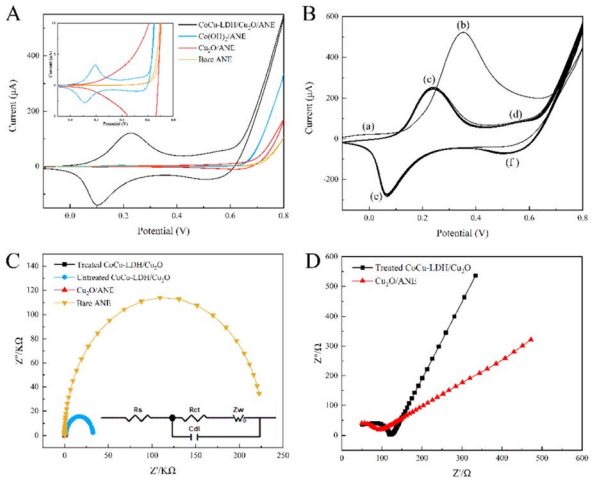

Fig. 4 (A) The CV curves of bare ANE, Cu_2O/ANE, $Co(OH)_2$/ANE, CoCu-LDH/Cu_2O/ANE in 0.1 M NaOH solution with a scan rate of 30 mV s^{-1} V (inset: magnified plot), and (B) the effect of CV scanning on CoCu-LDH/Cu_2O/ANE. (C) EIS of different electrodes at higher frequencies, and (D) EIS of Cu_2O/ANE and treated CoCu-LDH/Cu_2O/ANE in the solution of 20 mM $[Fe(CN)_6]^{3-/4-}$ and 0.1 M KCl.

Cu^{2+}/Cu^{3+} transition:

$$Cu_2O + 2OH^- \rightleftharpoons 2CuO + H_2O + 2e^- \quad (2)$$

Cu^{2+}/Cu^{3+} transition:

$$CuO + OH^- \rightleftharpoons CuOOH + e^- \quad (3)$$

Co^{2+}/Co^{3+} transition:

$$Co(OH)_2 + OH^- \rightleftharpoons CoOOH + H_2O + e^- \quad (4)$$

Co^{3+}/Co^{4+} transition:

$$CoOOH + OH^- \rightleftharpoons CoO_2 + H_2O + e^- \quad (5)$$

These results indicated that cauliflower-type Cu_2O NPs induced an increase in current density mainly by increasing the surface porosity and charge transfer.

Fig. 4B showed the effect of CV scanning cycle number on CoCu-LDH/Cu_2O/ANE in 0.1 M sodium hydroxide solution. In the first cycle, two peaks located at - 0.01 V (a) and 0.352 V (b) could be observed. The peak (a) was attributed to the adsorption of oxygen-containing chemicals such as OH^- on the electrode surface, and the peak (b) could be associated with the production of $Co(OH)_2$, CoOOH and CoO_2 under alkaline conditions.[59] By repeating 40 scans, two pairs of redox peaks (*c*/*e*) and (*d*/*f*) appeared, possibly indicating the conversion of Co(II)/Co(III) and Co(III)/Co(IV), respectively.[60]

The EIS generally consisted of a semicircular part at higher frequencies corresponding to the electron transfer limitation process and a linear part at lower frequencies corresponding to the diffusion process.[61] Therefore, the electron transfer resistance could be determined by measuring the semicircular diameter at higher frequencies in the EIS. As shown in Fig. 4C, the semicircular diameter of the bare ANE was significantly larger than that of the other electrodes at about 236 kΩ, indicating its large charge transfer resistance (R_{ct}). After the electrodeposition of Cu_2O NPs, R_{ct} significantly decreased to 65 Ω. The R_{ct} of untreated CoCu-LDH/Cu_2O/ANE suddenly increased to 31 kΩ which was due to some irregular CoCu-LDH nanosheets stacking on the electrode surface. But the R_{ct} significantly decreased to 91 Ω again after CV treatment of CoCu-LDH/Cu_2O/ANE in 0.1 M sodium hydroxide solution, which might be due to reconfiguration of the fast electron transport pathway by the conversion of Co(II)/Co(III) and Co(III)/Co(IV) with Cu_2O on the electrode surface. Besides that, CoCu-LDH/Cu_2O/ANE showed a greater slope compared with that of Cu_2O/ANE, indicating that CoCu-LDH/Cu_2O/ANE was less resistance to electron diffusion (Fig. 4D).

The electrochemical active surface area (ECSA) of CoCu-LDH/Cu_2O/ANE was also evaluated to better understand its actual electrocatalytic performance. Usually, the ECSA of electrode materials is calculated from the double-layer capacitance (C_{dl}),[62] which can be measured by CV in 0.1 M sodium hydroxide solution at different scan rates (10 to 100 mV s^{-1}) in the non-Faraday potential region from 0.3 V to 0.4 V (Fig. 5A–C). Here, the C_{dl} value can be calculated from half of the linear slope of the $\Delta J = J_a - J_c$ curve at 0.35 V, according to the following equation:

$$C_{dl} = \frac{1}{2}\frac{\Delta j}{\Delta v} \quad (6)$$

As shown in Fig. 5D, the C_{dl} value of Cu_2O/ANE was about 287.64 times higher than that of the bare ANE. After CV treatment in an alkaline solution, the C_{dl} value of CoCu-LDH/Cu_2O/ANE continued to be promoted and showed about 5.59 times higher than that of the Cu_2O/ANE.

Ultimately, the ECSA can be calculated by the following equation, in which C_S is the capacitance of a flat and uniform

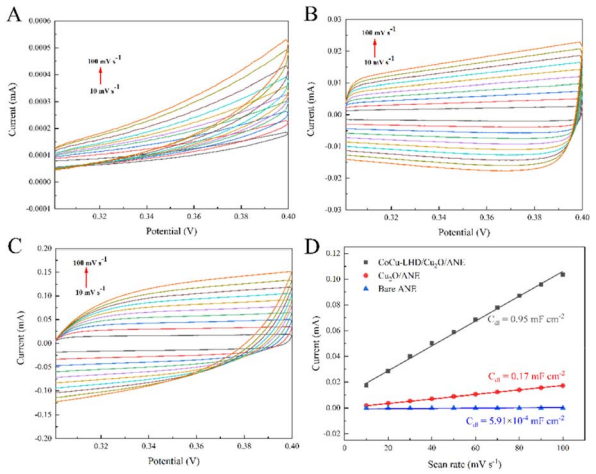

Fig. 5 CVs of the (A) bare ANE, (B) Cu_2O/ANE and (C) CoCu-LDH/Cu_2O/ANE in 0.1 M sodium hydroxide solution. (D) Double-layer capacitances (C_{dl}) of bare ANE, Cu_2O/ANE and CoCu-LDH/Cu_2O/ANE in 0.1 M NaOH solution.

surface with a real surface area of 1 cm^2 that corresponding to the literature,[63] and the assumed value of C_S is 0.04 mF cm^{-2} per cm^2 of ECSA:[64,65]

$$\mathrm{ECSA} = \frac{C_{dl}}{C_S} \quad (7)$$

The calculated value of ECSA for CoCu-LDH/Cu_2O/ANE was 23.75 cm^2, while the value for the Cu_2O/ANE was only 4.25 cm^2. This phenomenon suggested that CoCu-LDH/Cu_2O/ANE can provide more electroactive centers and higher electrocatalytic performance for the glucose molecules on the electrode surface.

Electrochemical behavior and sensing mechanism of glucose at CoCu-LDH/Cu_2O/ANE

The electrochemical behavior and sensing mechanism of ANE and its fabricated form toward glucose oxidation were assessed by CV measurements. As shown in Fig. 6A, bare ANE, Cu_2O/ANE and $Co(OH)_2$/ANE all exhibited electrocatalytic activity towards 4 mM glucose in 0.1 M sodium hydroxide solution, and Cu_2O/ANE was one of the best. It was probably due to the high specific surface area provided by the cauliflower-type Cu_2O NPs. Subsequently, the intensity of the CoCu-LDH/Cu_2O/ANE oxidation anode peak increased significantly, which confirmed the bimetallic synergism on the electrocatalytic activity of glucose because of the mixed valence of Cu/Co. Besides that, the neatly arranged CoCu-LDH nanosheets not only formed a porous network structure on the ANE surface but also provided NO_3^- and OH^- in the LDH interlayer, further facilitating the chemicals diffusion and electron transfer. The possible mechanism of glucose oxidation at CoCu-LDH/Cu_2O/ANE is shown in below:[66]

$$2CuOOH + C_6H_{12}O_6 = 2CuO + 2H_2O + C_6H_{10}O_6 \quad (8)$$

$$2CoOOH + C_6H_{12}O_6 = 2Co(OH)_2 + C_6H_{10}O_6 \quad (9)$$

$$2CoO_2 + C_6H_{12}O_6 = 2CoOOH + C_6H_{10}O_6 \quad (10)$$

Gluconolactone, an intermediate of glucose oxidation, was generated rapidly on the surface of the prepared CoCu-LDH network structures, and thus showing much higher oxidation current than reduction current.[67]

Fig. 6B showed the CV curves of CoCu-LDH/Cu_2O/ANE in the presence of different glucose concentrations (0–8 mM), and it was observed that the peak current around 0.5 V increased proportionally with the elevated concentration of glucose.

In addition, the kinetic mechanism of CoCu-LDH/Cu_2O/ANE was investigated by CV measurements at different scan rates from 10 to 100 mV s^{-1} in the presence of 4 mM glucose. As shown in Fig. 7A, the response current increased with the elevated scan rate. Fig. 7B showed a good linear relationship between the anodic currents and the scan rates, which suggested that the electrocatalytic oxidation of glucose by CoCu-LDH/Cu_2O/ANE was a typical surface-controlled adsorption process.

Optimization of variables for CoCu-LDH/Cu_2O/ANE

The development of efficient sensors requires the systematic study and optimization of analytical conditions such as electrodeposition potential and time, materials concentration for electrode preparation and working potential. CV measurement was performed and the corresponding current difference (ΔIp) on CoCu-LDH/Cu_2O/ANE was recorded in the presence of 4 mM glucose. As shown in Fig. S1,† the value of ΔI_p increased significantly with the rise of electrodeposition potential and time. The reason might be attributed to increasing the number of metal NPs deposited on the electrode to increase the specific surface and electrical conductivity of ANE. The value of ΔI_p started to decrease when the deposition potential and time increased to a certain extent, which could be attributed to the stacked Cu_2O NPs and thickened CoCu-LDH preventing the diffusion of glucose. Therefore, the optimum electrodeposition potential and time for Cu_2O NPs were set at −0.5 V and 250 s, and the optimum electrodeposition parameters for CoCu-LDH were −0.65 V and 200 s. Longer time (350 s) for CoCu-LDH electrodeposition was also tested, and the FE-SEM results were shown in Fig. S2.† Obviously, the CoCu-LDH thickness increased with the time prolongation, which result highly in coincidence with our conclusion.

Afterward, the effect of $CuSO_4$ concentration on the electrochemical catalysis of CoCu-LDH/Cu_2O/ANE towards glucose was investigated, as shown in Fig. S3A.† When the $CuSO_4$ concentrations changed from 20 to 50 mM, the peak currents of CoCu-LDH/Cu_2O/ANE increased accordingly. When continued to increase the $CuSO_4$ concentrations from 60 to 80 mM, the

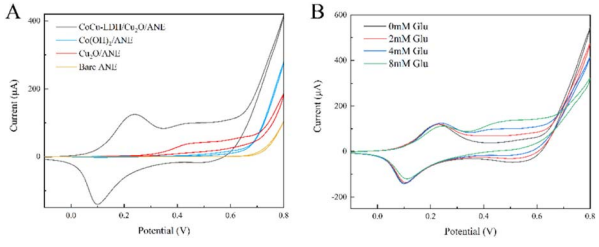

Fig. 6 (A) The CV curves of bare ANE, Cu_2O/ANE, $Co(OH)_2$/ANE, and CoCu-LDH/Cu_2O/ANE in the presence of 4 mM glucose, and (B) the CV curves of CoCu-LDH/Cu_2O/ANE at different glucose concentrations.

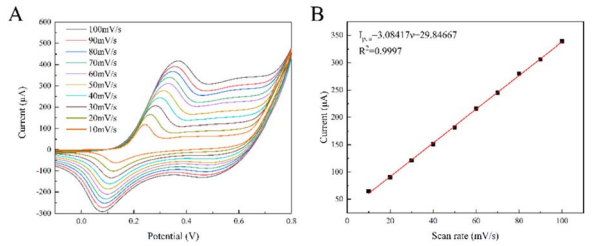

Fig. 7 (A) The CV curves of CoCu-LDH/Cu_2O/ANE in the presence of 4 mM glucose at different scan rates, and (B) the plot of oxidation peak currents *versus* scan rates.

currents decreased significantly. In Fig. S3B,† the effect of $Co(NO_3)_2/CuSO_4$ molar ratio on the electrochemical catalysis of CoCu-LDH/Cu_2O/ANE for glucose was explored. To combine the results from Fig. 6A and S3B,† the contact interface of CoCu-LDH/Cu_2O bimetal was identified as an important electrocatalytic center for glucose oxidation, and the prepared CoCu-LDH/Cu_2O exhibited the highest electrocatalytic activity when the molar ratio of $Co(NO_3)_2/CuSO_4$ was 1 : 1.

It is widely known that lower potentials can lead to incomplete oxidation of glucose, which affects the sensitivity of the designed sensor significantly. On the contrary, an abuse of higher potential can lead to a lower selectivity of the sensor because some interfering substances may be oxidized.[68,69] Fig. S3C† showed the amperometric current–time (*i*–*t*) curves of the CoCu-LDH/Cu_2O/ANE sensor under the different applied potentials (0.40 V, 0.45 V, 0.5 V, 0.55 V, and 0.60 V) with the continuous addition of 0.2 mM glucose in 0.1 M NaOH. It was found that the current response of the sensor increased originally and then decreased with the elevated potential. This phenomenon might be involved in the oxidation of O^{2-} to O_2 and the separation of some electroactive sites from CoCu-LDH/Cu_2O/ANE at the higher potential of 0.60 V. Therefore, 0.55 V was chosen as the optimum potential to further study the sensing characteristics of the designed CoCu-LDH/Cu_2O/ANE sensor.

Investigation on typical sensing performances of CoCu-LDH/Cu_2O/ANE

The performances such as sensitivity, linear detection range, detection limit, selectivity, and electrochemical stability are key parameters of electrochemical sensors and therefore must be carefully explored before the construction of a non-enzymatic electrochemical platform for glucose. To this end, the amperometric test has been extensively used as an electrochemical tool to study the characteristics of the modified working electrode.[70] Fig. 8A showed the *i*–*t* curves of CoCu-LDH/Cu_2O/ANE with continuous addition of glucose solution into a continuously stirred 0.1 M NaOH solution at 0.55 V. As can be seen, the working electrode had an obvious response and was easy to reach the steady state within 3 s after continuous additions of glucose. The calibration curve of CoCu-LDH/Cu_2O/ANE was obtained by plotting the current response *I* (μA) *versus* glucose concentration *c* (mM) as shown in Fig. 8B.

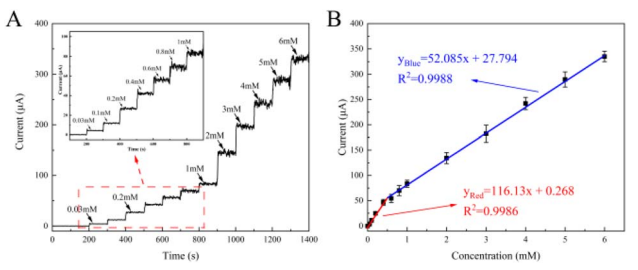

Fig. 8 (A) The *i*–*t* curves of CoCu-LDH/Cu_2O/ANE in 0.1 M NaOH with continuous addition of glucose solution at 0.55 V (the inset is the low-concentration region of glucose), and (B) the linear calibration curves of current response *versus* glucose concentration.

The results showed two linear ranges from 0.03 to 0.40 mM and another from 0.40 to 6.00 mM, according to the following regression equation:

For the range of 0.03 to 0.40 mM:

$$y_{Red} = 116.13x + 0.268 \ (R^2 = 0.9986) \quad (11)$$

For the range of 0.40 to 6.00 mM:

$$y_{Blue} = 52.085x + 27.794 \ (R^2 = 0.9988) \quad (12)$$

The sensitivity in the two linear ranges was 116.13 μA mM^{-1} and 52.08 μA mM^{-1}, respectively. The decrease in sensitivity at higher glucose concentrations might be related to the strong adsorption of intermediates generated by the electrooxidation of glucose on the electrode surface, which resulted in fewer electroactive sites for the catalytic oxidation of glucose. The detection limit of our glucose sensor based on CoCu-LDH/Cu_2O/ANE had been proven to be as low as 0.46 μM (S/N = 3). Compared with the performance of glucose sensors reported in the literature (Table S1†), our sensor provided a comparable or even better sensing performance in terms of lower detection limit and satisfactory sensitivity.

For an enzyme-free sensing system, selectivity is a vital indicator for measuring the sensing performance. In this regard, the common interferences including AA, DA, UA and Cl^- were detected with the amperometric method in 0.1 M NaOH solution. The molar ratio of glucose to interferences was 10 : 1 to simulate the physiological condition. As shown in Fig. S4A,† the amperometric current increased obviously after the addition of 0.5 mM glucose. Subsequently, the current increased less than one-tenth to respond to the addition of 0.05 DA. However, there was almost no disturbance in the amperometric current with successive addition of 0.05 mM AA, UA and Cl^-. All results proved that the fabricated CoCu-LDH/Cu_2O/ANE had excellent properties not only in selectivity but also in anti-poisoning Cl^-.

The reproducibility of CoCu-LDH/Cu_2O/ANE was also investigated by measuring the CV current response of five fabricated electrodes in 0.1 M sodium hydroxide solution containing 4 mM glucose, and the relative standard deviation (RSD) of the current for five parallel experiments was 2.12% (shown in Fig. S4B†).

The stability plays an important role in the sensor applications. Therefore, the long-term stability of CoCu-LDH/Cu_2O/ANE was assessed by storing it in a closed desiccator at room temperature and testing its changes of electrocatalytic current for glucose over a period of 15 days. As shown in Fig. S4C,† the currents decreased slowly and still retained 93.08% current intensity as compared with the original current after 15 days. The morphology changes of CoCu-LDH/Cu_2O/ANE that had been reused 4 times in 15 days were shown in Fig. S4D.† CoCu-LDH generally remained the initial conformations but glucose oxidation products might be left on the surface of CoCu-LDH/Cu_2O/ANE, which was the reason for only a slight decrease in current. These results confirmed that CoCu-LDH/Cu_2O/ANE

Table 1 Determination and recovery of glucose detection in spiked human serum samples, using CoCu-LDH/Cu_2O/ANE sensor

Sample	Determined (mM)	Added (mM)	Found (mM)	RSD (%)	Recovery (%)
1	0.498	0.00	0.49	1.78	
		0.40	0.90	1.47	101.13
		0.80	1.29	1.32	99.42
		1.20	1.68	1.23	98.66
2	0.518	0.00	0.51	1.53	
		0.50	1.02	1.42	100.28
		1.00	1.52	1.46	100.62
		1.50	2.01	1.25	99.54

had a good long-term stability, even though there were problems of the temperature fluctuation in the storage environment.

Real sample analysis

To further validate the practical application of the CoCu-LDH/Cu_2O/ANE sensor, the fabricated electrode was used to detect glucose in human serum samples. The samples were collected from two volunteers with known concentrations and then diluted 10 times with 0.1 M NaOH solution. It was clearly seen that the results detected by the CoCu-LDH/Cu_2O/ANE sensor were more similar to these provided by the hospital (Women and Children's Hospital of Jinzhou) than they were to the results detected by a commercially available blood glucose meter (Table S2†). As shown in Table 1, the spiked recoveries and RSDs were acceptable in the ranges of 98.66–101.13% and 1.23–1.78%, respectively, further indicating that the fabricated sensor based on CoCu-LDH/Cu_2O/ANE had a favorable potential for clinical application and daily blood glucose monitoring.

Conclusions

In summary, CoCu-LDH/Cu_2O 3D porous nanohybrid structures had been successfully synthesized on the tip surface and used for highly sensitive and selective electrochemical sensing towards glucose. The Cu-based CoCu-LDH composites with special morphology accelerated the electron transport and provided sufficient active centers for the electrocatalytic process. Besides that, the mixed valence of Cu/Co further improved the electrochemical sensing performance of glucose. As a result, the glucose sensor based on CoCu-LDH/Cu_2O/ANE showed two wider linear ranges of 0.03–0.40 mM and 0.40–6.00 mM, and the corresponding sensitivities were 116.13 μA mM^{-1} and 52.08 μA mM^{-1}, respectively, with rapid response time as low as 3 s, good reproducibility, and low detection limit (0.46 μM). In addition, the CoCu-LDH/Cu_2O/ANE sensor possessed a good anti-interference capacity and could be used in human serum samples. Until now, diluting samples in the alkaline solution is still a problem that troubles us, but through improvement of material preparing technology and composition, functionalized microneedle based on bimetal-LDH has a great prospect in exploration of more comfortable puncture experience, simple, economical, highly sensitive and selective sensors for small and micro-volume sampling and detection.

Informed consent

Informed consents were obtained from human participants of this study.

Author contributions

Jialei Zhu: experimental design and implementation, original draft preparation, and data analysis. Fuqin Wang: original draft preparation and data analysis. Jiayi Chen: data analysis. Chang Liu: validation, reply to editor and reviewer, and funding support.

Conflicts of interest

There are no conflicts to declare.

Acknowledgements

This work is supported by the Liaoning Province Department of Education Fund (JYTJCZR2020069).

References

1 N. Zhang, J. Zhou, W. Su, J. Yang, Z. Zhu, Y. Liu and P. Wang, *Microchem. J.*, 2023, 189.
2 Y. Zhang, P. Xia, H. Fan, X. Gao, F. Ouyang and W. Chen, *Dalton Trans.*, 2023, **52**, 2603–2610.
3 Z. Yu, H. Wu, Z. Xu, Z. Yang, J. Lv and C. Kong, *Sensors*, 2023, 23.
4 T. Chen, D. Liu, W. Lu, K. Wang, G. Du, A. M. Asiri and X. Sun, *Anal. Chem.*, 2016, **88**, 7885–7889.
5 M. Wei, Y. Qiao, H. Zhao, J. Liang, T. Li, Y. Luo, S. Lu, X. Shi, W. Lu and X. Sun, *Chem. Commun.*, 2020, **56**, 14553–14569.
6 J. Pang, K. Sun, S. Jin, J. Hou, G. Wang, K. Sun, Y. Zheng, Y. Zhang and L. Chen, *Chem. Eng. J.*, 2023, 454.
7 V. Vediyappan, M. Sivakumar, S.-M. Chen, Q. Lai and R. Madhu, *J. Alloys Compd.*, 2021, 875.
8 R. Li, X. Liu, H. Wang, Y. Wu, K. C. Chan and Z. Lu, *Electrochim. Acta*, 2019, **299**, 470–478.
9 K. M. Saifullah and Z. Faraji Rad, *Adv. Mater. Interfaces*, 2023, **10**, 2201763.
10 N. M. Nor, N. S. Ridhuan and K. A. Razak, *Biosensors*, 2022, **12**, 1136.
11 A. Bisht, A. Mishra, H. Bisht and R. M. Tripathi, *J. Anal. Test.*, 2021, **5**, 327–340.
12 M. Chongbo and Z. Ming, *Chin. J. Anal. Chem.*, 2022, **50**, 535–544.
13 X. Liu, F. He, L. Bai, X. Cao, C. Liu and W. Lu, *Anal. Chim. Acta*, 2022, 1210.
14 P. Tetyana, N. Mphuthi, A. N. Jijana, N. Moloto, P. M. Shumbula, A. Skepu, L. S. Vilakazi and L. Sikhwivhilu, *Nanomaterials*, 2023, **13**, 481.
15 J. Cao, J. Yun, N. Zhang, Y. Wei, H. Yang and Z. Xu, *Synth. Met.*, 2021, 282.
16 Y. Qiao, Q. Liu, S. Lu, G. Chen, S. Gao, W. Lu and X. Sun, *J. Mater. Chem. B*, 2020, **8**, 5411–5415.

17 Y.-H. Lin, C. Sivakumar, B. Balraj, G. Murugesan, S. K. Nagarajan and M.-S. Ho, *Nanomaterials*, 2023, 13.
18 V. Z. Zulfa, N. Nasori, U. Farahdina, M. Firdhaus, I. Aziz, H. Suprihatin, M. N. Rhomadhoni and A. Rubiyanto, *Molecules*, 2023, 28.
19 M. Waqas, L. Yang, Y. Wei, Y. Sun, F. Yang, Y. Fan and W. Chen, *Electrochim. Acta*, 2023, 440.
20 M. Baghayeri, M. Nodehi, A. Amiri, N. Amirzadeh, R. Behazin and M. Z. Iqbal, *Anal. Chim. Acta*, 2020, **1111**, 49–59.
21 W. Liu, Q. Guo, X. Zhao, B. Zhang, M. Wang, Y. Dai and Y. Qi, *Colloids Surf., B*, 2021, 208.
22 L. Bai, Y. Shi, X. Zhang, X. Cao, J. Jia, H. Shi and W. Lu, *Analyst*, 2023, **148**, 3359–3370.
23 F. Xie, X. Cao, F. Qu, A. M. Asiri and X. Sun, *Sens. Actuators, B*, 2018, **255**, 1254–1261.
24 A. Mustafa, I. A. Alsafari, H. H. Somaily, S. Yousaf, M. I. Din, J. Rahman, M. Shahid, M. Ashraf and M. F. Warsi, *Phys. B*, 2023, 648.
25 L. Naderi, S. Shahrokhian, M. K. Amini and M. H. Kahnamouei, *ACS Appl. Nano Mater.*, 2023, **6**, 2755–2769.
26 Z. Wang, X. Cao, D. Liu, S. Hao, R. Kong, G. Du, A. M. Asiri and X. Sun, *Chem. Eur. J.*, 2017, **23**, 4986–4989.
27 L. Li, J. Long, Q. Ye, X. Xu and F. Wang, *J. Alloys Compd.*, 2023, 946.
28 C. Mousty and H. Farhat, *Electroanalysis*, 2023, **35**, e202200527.
29 S. Kwon, J. Zhang, R. Ganganahalli, S. Verma and B. S. Yeo, *Angew. Chem., Int. Ed.*, 2023, **62**, e202217252.
30 D. Zhai, J. Wen, Q. Ding, Y. Feng and W. Yang, *Int. J. Hydrogen Energy*, 2023, **48**, 10108–10117.
31 A. V. Karim, A. Hassani, P. Eghbali and P. V. Nidheesh, *Curr. Opin. Solid State Mater. Sci.*, 2022, **26**, 100965.
32 Y. Cong, T. Jiang, Y. Dai, X. Wu, M. Lv, M. Chen, T. Ye and Q. Wu, *Mater. Res. Bull.*, 2023, 157.
33 F. L. Bohari, S. A. I. S. M. Ghazali, N. N. Dzulkifli, S. N. A. Baharin, I. Fatimah and S. Poddar, *Open Chem.*, 2023, 21.
34 Y. Yang, X. Du, A. Abudula, Z. Zhang, X. Ma, K. Tang, X. Hao and G. Guan, *Sep. Purif. Technol.*, 2019, **223**, 154–161.
35 Y. Cao, D. Zheng, F. Zhang, J. Pan and C. Lin, *J. Mater. Sci. Technol.*, 2022, **102**, 232–263.
36 W. Jang, J. Kim, S. Yoon, M. Kim, J. Kim, K. An and S. Cho, *Small Struct.*, 2023, **4**, 2200279.
37 H. Jiang, Q. Ke, X. Qiu, J. Chen, P. Chen, S. Wang, X. Luo and B. Rao, *Inorg. Chem. Front.*, 2023, **10**, 2154–2164.
38 P. Dardano, I. Rea and L. De Stefano, *Curr. Opin. Electrochem.*, 2019, **17**, 121–127.
39 Y. Zhou, F. Ding, G.-J. Zhang, L.-N. Tang and Y.-T. Li, *Chin. J. Anal. Chem.*, 2021, **49**, 35–40.
40 C. Xu, C. Gu, Q. Xiao, J. Chen, Z.-Z. Yin, H. Liu, K. Fan and L. Li, *Chem. Eng. J.*, 2022, 436.
41 C. Tortolini, A. E. G. Cass, R. Pofi, A. Lenzi and R. Antiochia, *Microchim. Acta*, 2022, 189.
42 P. Li, M. Ge, D. Lin and L. Yang, *Anal. Bioanal. Chem.*, 2019, **411**, 5669–5679.
43 H. Jia, J. Zhao, L. Qin, M. Zhao and G. Liu, *RSC Adv.*, 2019, **9**, 26843–26849.
44 Y. Li, H. Han, D. Pan and P. Zhang, *J. Electrochem. Soc.*, 2019, **166**, B1038–B1043.
45 S. M. M. Dhanjai and W. Lu, *Anal. Bioanal. Chem.*, 2020, **412**, 7063–7072.
46 H. Dang, X. Dong, Y. Dong, H. Fan and Y. Qiu, *Mater. Lett.*, 2015, **138**, 56–59.
47 D. Chen, L. Tian, C. Yin, Y. Liu, Q. Fu and C. Li, *Sens. Actuators, B*, 2020, 323.
48 D.-P. Sui, H.-X. Chen, L. Liu, M.-X. Liu, C.-C. Huang and H.-T. Fan, *Talanta*, 2016, **148**, 285–291.
49 S. Eyupoglu, *J. Nat. Fibers*, 2022, **19**, 1287–1296.
50 S. Wang, W. Xu, D. Zeng, R. Zhang and T. Shu, *J. Mater. Sci.*, 2023, **58**, 199–210.
51 F. Gao, J. Wang, M. Jiang, X. Du, X. Ma, X. Hao, X. Yue and G. Guan, *Sep. Purif. Technol.*, 2021, 265.
52 X. Zheng, X. Han, X. Zhao, J. Qi, Q. Ma, K. Tao and L. Han, *Mater. Res. Bull.*, 2018, **106**, 243–249.
53 J. Sun, A. Song, Y. Tian, H. Zhan, J. Deng, H. Wang and M. Ke, *Chemcatchem*, 2023.
54 L. Wang, C. Lin, F. Zhang and J. Jin, *Acs Nano*, 2014, **8**, 3724–3734.
55 Z. Ren, R. Dong and Y. Liu, *Nanotechnology*, 2022, 33.
56 F. Hu, B. Song, X. Wang, S. Bao, S. Shang, S. Lv, B. Fan, R. Zhang and J. Li, *Chin. Chem. Lett.*, 2022, **33**, 308–313.
57 W. Li, S. Lv, Y. Wang, L. Zhang and X. Cui, *Sens. Actuators, B*, 2019, **281**, 652–658.
58 A. A. Saleh, A. Amer, D. M. Sayed and N. K. Allam, *Electrochim. Acta*, 2021, 380.
59 M. Pak, A. Moshaii, H. Siampour, S. Abbasian and M. Nikkhah, *Microchim. Acta*, 2020, 187.
60 T. Wang, Y. Yu, H. Tian and J. Hu, *Electroanalysis*, 2014, **26**, 2693–2700.
61 S. Shahrokhian, L. Naderi and M. Ghalkhani, *Mater. Sci. Eng. C*, 2016, **61**, 842–850.
62 L. Naderi and S. Shahrokhian, *Nanoscale*, 2022, **14**, 9150–9168.
63 X. Wang, L. Yu, B. Y. Guan, S. Song and X. W. Lou, *Adv. Mater.*, 2018, **30**.
64 H. Deng, C. Zhang, Y. Xie, T. Tumlin, L. Giri, S. P. Karna and J. Lin, *J. Mater. Chem. A*, 2016, **4**, 6824–6830.
65 M. A. Kachouei, S. Shahrokhian and M. Ezzati, *Sens. Actuators, B*, 2021, 344.
66 X. Xiao, S. Zheng, X. Li, G. Zhang, X. Guo, H. Xue and H. Pang, *J. Mater. Chem. B*, 2020, **8**, 5547–5548.
67 L. Naderi and S. Shahrokhian, *Chem. Eng. J.*, 2023, 456.
68 L.-N. Wu, J.-P. Zhong, M. Waqas, Z. Jiang, Y.-J. Fan, Y. Sun, J. Li and W. Chen, *Electrochim. Acta*, 2019, **318**, 837–846.
69 M. Waqas, C. Liu, Q. Huang, X. Zhang, Y. Fan, Z. Jiang, X. Wang and W. Chen, *Electrochim. Acta*, 2022, 410.
70 V. Archana, Y. Xia, R. Fang and G. G. Kumar, *ACS Sustainable Chem. Eng.*, 2019, **7**, 6707–6719.